ON CRACK INTERACTION EFFECTS OF IN-PLANE SURFACE CRACKS USING ELASTIC AND ELASTIC-PLASTIC FINITE ELEMENT ANALYSES

JONG-MIN KIM[1] and NAM-SU HUH[2,*]
[1]Department of Mechanical Engineering, Sungkyunkwan University
300 Chunchun-dong, Jangan-gu, Suwon 440-746, Korea
[2]School of Mechanical Design and Automation Engineering
Seoul National University of Science and Technology
172 Gongreung 2-dong, Nowon-gu, Seoul 139-743, Korea
[*]Corresponding author. E-mail : nam-su.huh@seoultech.ac.kr

Received August 02, 2010
Accepted for Publication November 04, 2010

The crack-tip stress fields and fracture mechanics assessment parameters for a surface crack, such as the elastic stress intensity factor or the elastic-plastic *J*-integral, can be affected significantly by the adjacent cracks. Such a crack interaction effect due to multiple cracks can alter the fracture mechanics assessment parameters significantly. There are many factors to be considered, for instance the relative distance between adjacent cracks, the crack shape, and the loading condition, to quantify the crack interaction effect on the fracture mechanics assessment parameters. Thus, the current assessment codes on crack interaction effects (crack combination rules), including ASME Sec. XI, BS7910, British Energy R6 and API 579-1/ASME FFS-1, provide different rules for combining multiple surface cracks into a single surface crack. The present paper investigates crack interaction effects by evaluating the elastic stress intensity factor and the elastic-plastic *J*-integral of adjacent in-plane surface cracks in a plate through detailed 3-dimensional elastic and elastic-plastic finite element analyses. The effects on the fracture mechanics assessment parameters of the geometric parameters, the relative distance between two cracks, and the crack shape are investigated systematically. As for the loading condition, an axial tension is considered. Based on the finite element results, the acceptability of the crack combination rules provided in the existing guidance was investigated, and the relevant recommendations on a crack interaction for in-plane surface cracks are discussed. The present results can be used to develop more concrete guidance on crack interaction effects for crack shape characterization to evaluate the integrity of defective components.

KEYWORDS : Crack Interaction Effect, Crack Proximity Rule, Finite Element Analysis, In-Plane Surface Cracks, *J*-Integral, Multiple Cracks, Plate, Stress Intensity Factor

1. INTRODUCTION

For the structural integrity assessment or remaining life estimation of components containing defects, defects that were detected during an in-service inspection must be represented by an equivalent plane crack-like defect before they are assessed by using the fracture mechanics concepts. In the case of a surface crack, each surface crack is characterized as a semi-elliptical crack or a semi-circular crack. In general, during an in-service inspection, if many multiple cracks have been found, the crack-tip stress fields and the fracture mechanics assessment parameters for a surface crack, such as the elastic stress intensity factor and the elastic-plastic *J*-integral [1], can be affected significantly by adjacent cracks. Such a crack interaction effect due to adjacent cracks can magnify the fracture mechanics assessment parameters. Therefore, crack interaction effects should be taken into account and these cracks should also be treated as a single crack when the interaction effects are significant. However, there are many factors that must be considered in order to quantify the effect of crack interaction on the fracture mechanics assessment parameters, for instance the distance between cracks, the crack geometry, and the loading condition, and the complexity of these considerations makes it very challenging to develop concrete assessment rules. In this context, the existing integrity assessment codes on crack interaction effects, including ASME Sec. XI [2], API

579-1/ASME FFS-1 [3] and BS7910 [4], provide different rules for combining multiple surface cracks into a single surface crack. British Energy R6 [5] uses the same combination rule for a crack interaction effect as BS7910.

In order to provide concrete guidance on crack interaction effects, 3-dimensional (3-D) finite element (FE) analyses must be employed. However, 3-D FE analyses for multiple surface cracks pose difficulties due to their geometric complexity. Murakami et al. [6] investigated the elastic stress intensity factor of interacting surface cracks based on the body force method, and the line spring model was invoked to analyze the elastic stress intensity factor of twin semi-elliptical cracks in tension by Miyoshi et al. [7]. Hasegawa et al. [8] evaluated the conservatism of the crack combination rule in ASME Sec. XI based on existing analytical stress intensity factor solutions for various crack shapes, and Kamaya [9] also evaluated a variation of the elastic stress intensity factor for interacting semi-elliptical surface cracks for limited geometries using a finite element alternating method. As mentioned above, although many analytical and numerical attempts have been made to investigate the crack interaction effects of multiple cracks, little attempt has been made to investigate these interaction effects systematically using a detailed 3-D FE analysis for improved accuracy.

Based on detailed 3-D, elastic and elastic-plastic FE analyses, the present paper quantifies the crack interaction effects of two adjacent in-plane surface cracks in a plate. As for the loading condition, an axial tension was considered. The geometric variables affecting the crack interactions were considered systematically. Particularly, the trend of crack interaction effects due to different crack aspect ratios (different crack shapes) was systematically investigated. Based on the FE results, the elastic stress intensity factors and the elastic-plastic *J*-integral along the crack front were obtained. Variations of not only the maximum stress intensity factor and the *J*-integral values but also both parameters at the maximum interacting point were evaluated. Moreover, the applicability and limitations of the current guidance for crack interaction effects (crack combination rule) were discussed based on the present FE results.

2. REVIEW OF THE GUIDANCE ON AN INTERACTION EFFECT

Figure 1 depicts multiple surface cracks (dual adjacent surface cracks) in a plane. In Fig. 1, a_1 and a_2 denote the crack depth of each crack, respectively, and c_1 and c_2 denote a half of a crack length of each crack, respectively. The distance between two adjacent cracks is characterized as S. As mentioned previously, there are several codes for crack combination rules that consider the crack interaction effect. When the combination rule of ASME Sec. XI is employed, the distance between two adjacent surface cracks, S, should be compared with half of the crack depth of each crack, max($0.5a_1$ and $0.5a_2$), for use in determining the allowable flaw size and for comparison with acceptance standards of IWB-3500, and if one of those values is equal to or greater than the distance between adjacent cracks, the cracks are combined as a single in-plane crack. On the other hand, API 579-1/ASME FFS-1, BS7910 and British Energy R6 use the length of each crack as an interaction criterion, and BS7910 provides different rules depending on the ratio of crack depth to crack length.

The crack interaction criterion of these codes is summarized as follows, where S_{min} denotes the minimum critical distance between adjacent cracks for combining cracks into a single crack.

$$\begin{aligned} &S_{min}=0.5\max(a_1, a_2) && \text{for ASME Sec. XI} \\ &S_{min}=c_1+c_2 && \text{for API 579-1/ASME FFS-1} \\ &S_{min}=0 \text{ if } c/a>1 \\ &\quad \text{or } 2\min(c_1, c_2) \text{ if } c/a<1 && \text{for BS7910 (and R6)} \end{aligned} \quad (1)$$

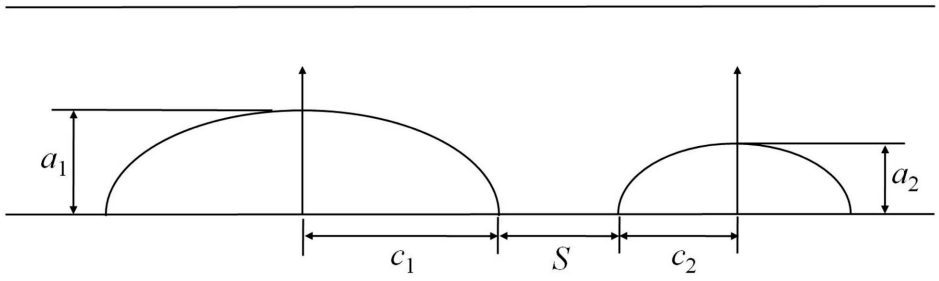

Fig. 1. Geometry of Dual Adjacent In-Plane Surface Cracks

Then, if $S<S_{min}$, an interaction of two in-plane surface cracks occurs, and thus a new single combined crack is re-characterized as

$$2c=2(c_1+c_2)+S,\ a=\max(a_1, a_2), \quad (2)$$

where c and a are half of the crack length and crack depth of the new single combined crack, respectively.

At this point, it should be noted that, when applying the crack characterization rule of ASME Sec. XI, IWA-3000 [2], the crack aspect ratio, i.e. c/a, shall not be less than 1. Thus, the crack aspect ratio (c/a) should be set as 1.0 if $c/a<1$ for the fracture assessment. In the present paper, the applicability and accuracy of the above combination rules were investigated by using a detailed elastic and elastic-plastic 3-D FE analysis.

3. FINITE ELEMENT ANALYSES

3.1 Geometry

Two geometries, i.e. plates with two adjacent surface cracks and with a single crack, were considered in the present study. Figure 2(a) shows a plate with two adjacent surface cracks where t, h, and w are the plate thickness, height and width, respectively. The plate was subjected to an axial tension load (σ^{∞}). The shape of the surface cracks was characterized by the crack length and the depth of each crack. The crack length was defined as c_1 and c_2 where $c_1>c_2$, and the depth was defined as a_1 and a_2 where $a_1>a_2$. The distance between cracks was denoted as S, and the definition of the crack angle ϕ along the crack front is given in Fig. 2(b).

The cases considered in the present study are listed in Table 1. In terms of the crack depth, the values of a_1/t and a_2/t were fixed at 0.5 and 0.3, respectively. In terms of the crack length, three different values for the ratio of

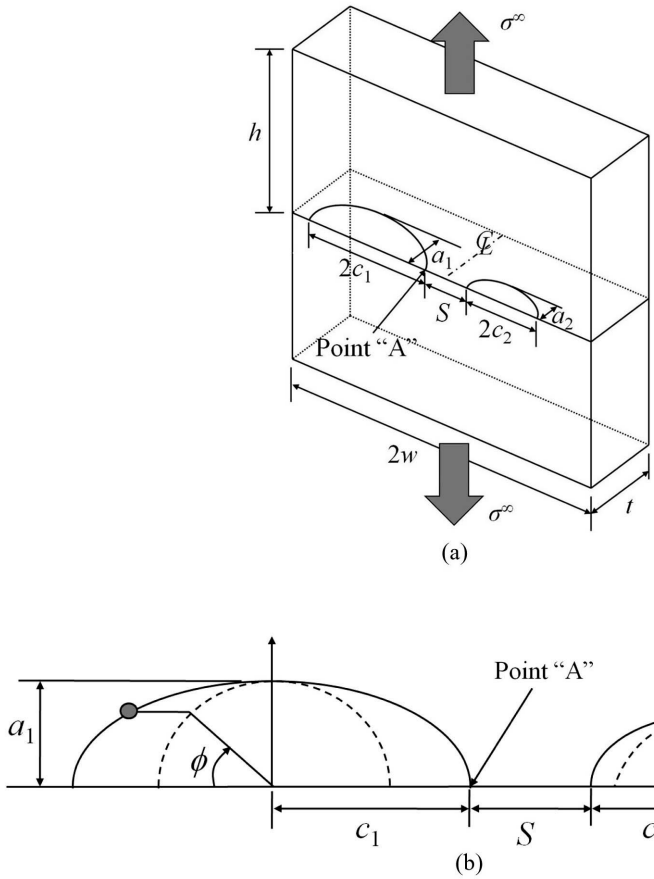

Fig. 2. (a) Schematic Illustration of Plate Containing Two Adjacent Surface Cracks Under Axial Tension and (b) Definition of the Crack Angle ϕ along the Crack Front

crack length to crack depth, c/a, were selected, $c_1/a_1=c_2/a_2=3$, 1 and 0.5, to investigate the effect of the crack aspect ratio on the interaction effects. Figure 3 shows the schematics of the crack shapes considered in the present study according to the crack aspect ratio, c/a. The critical distance (S_{min}) values between the adjacent cracks of each case in accordance with the current combination rules are also given in Table 1. Based on these S_{min} values of each case, three different values of S covering a range of all S_{min} resulting from the existing assessment codes were selected for each c/a, so that it can be expected that the most appropriate guidance for a crack interaction effect could be found. For all cases, w/t was set at a fixed value of 16 [10]. As noted previously, if $c/a<1.0$, the crack aspect ratio should be set as 1.0 in ASME Sec. XI, IWA-3000; thus, in the present study, the combination rule of ASME Sec. XI was not applied to the case of $c/a=0.5$.

Figure 4 depicts a plate with a single surface crack under an axial tension. For the single surface cracked plate, three different values of c_o/a_o (=3, 1, 0.5) were considered, and a_o/t was fixed at 0.5, which is equal to the size of a larger crack of a plate with dual surface cracks (see Table 1). Thus, the crack interaction effects due to adjacent cracks can be estimated by comparing the elastic stress intensity factors and the elastic-plastic J-integrals of the dual cracks with those of a single crack with the same size. Again, w/t was set as equal to 16 for all cases.

3.2 Finite Element Calculation

Elastic and elastic-plastic analyses of the FE models for the plates with dual surface cracks and a single surface crack, depicted in Fig. 2 and Fig. 4, were performed using the general-purpose FE program, ABAQUS [11]. The plate material was assumed to be homogeneous and isotropic. For the elastic analyses, the linear elastic material with a Poisson's ratio of 0.3 was used, and for the elastic-plastic analyses, the tensile properties for the FE analysis were assumed to follow the Ramberg-Osgood (R-O) idealization:

$$\frac{\varepsilon}{\varepsilon_o}=\frac{\sigma}{\sigma_y}+\alpha\left(\frac{\sigma}{\sigma_y}\right)^n, \quad (3)$$

where ε_o, σ_y, α and n are constants, with $E\varepsilon_o=\sigma_y$ where E is the Young's modulus. The deformation plasticity option with a small geometry change continuum model was invoked. The variables α and σ_y were fixed to $\alpha=1$ and $\sigma_y=400$MPa, and E and the strain hardening exponent n were selected as $E=200$GPa and $n=5$, respectively. These

Table 1. Cases Considered in the Present Study for Two Adjacent Surface Cracks

a_1/t	a_2/t	c_1/a_1, c_2/a_2	S	S_{min}
0.5	0.3	3	0.2t	API 579-1/ASME FFS-1: 2.4t ASME Sec. XI: 0.25t BS7910 (R6): 0
			2t	
			2.5t	
		1	0.2t	API 579-1/ASME FFS-1: 0.8t ASME Sec. XI: 0.25t BS7910 (R6): 0
			0.5t	
			t	
		0.5	0.2t	API 579-1/ASME FFS-1: 0.4t BS7910 (R6): 0.3t
			0.3t	
			0.5t	

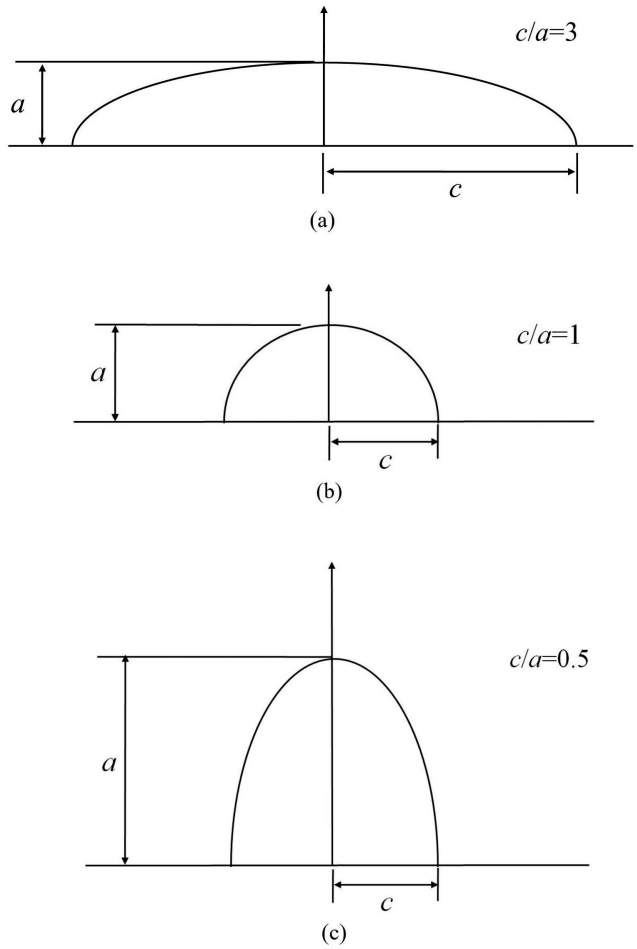

Fig. 3. Typical Crack Shapes Considered in the Present Study According to the Crack Aspect Ratio

elastic-plastic material properties are believed to be typical representative values for the material employed in the nuclear industry. Furthermore, the strain hardening exponent in the typical range (n=~10) does not produce a remarkable difference in the elastic-plastic behavior of the material.

A symmetric condition was applied, and thus only a half of a plate was modeled for the dual surface crack analysis and only a quarter of a plate was modeled for the single surface crack analysis. Figure 5 depicts the typical 3-D FE meshes employed in the present work, (a) for the plate with dual surface cracks and (b) for the plate with a single surface crack. Reduced integration 20-node brick isoparametric elements (element type C3D20R in the ABAQUS element library) were used. The number of elements and nodes in the FE mesh are 14956 elements/68700 nodes for the plate with dual surface cracks and 6688 elements/30539 nodes for the plate with a single surface crack. The crack-tip was modeled with a focused wedge type element with 5 contours. In terms of the loading condition, an axial tension was applied to a remote surface as a distributed load (σ^{∞}), as shown in Fig. 2 and Fig. 4. For the elastic-plastic analyses using the R-O material, the axial tension was applied up to a yield stress of $\sigma^{\infty}=\sigma_y$ (=400MPa).

The elastic and elastic-plastic J-integral values along the crack front were extracted directly from the FE results using a domain integral method embedded in ABAQUS as a function of the crack front angle, ϕ (see Fig. 2(b) and Fig. 4(b)). Note that when calculating the elastic J-integral to obtain the elastic stress intensity factor, the crack-tip nodes on the collapsed face were constrained to move together by using the MPC-TIE option within ABAQUS and the mid-side nodes were moved to the quarter points nearest to the crack-tip to simulate a relevant crack-tip singularity. Thus, path independence for an elastic FE J-integral was achieved within a maximum difference of 1%, and then the elastic J-integral was determined from the mean of the 2nd-5th contours.

The elastic stress intensity factor, K, was then determined from the elastic FE J-integral using the following equation.

$$K = \sqrt{\frac{EJ_e}{1-\nu^2}}, \tag{4}$$

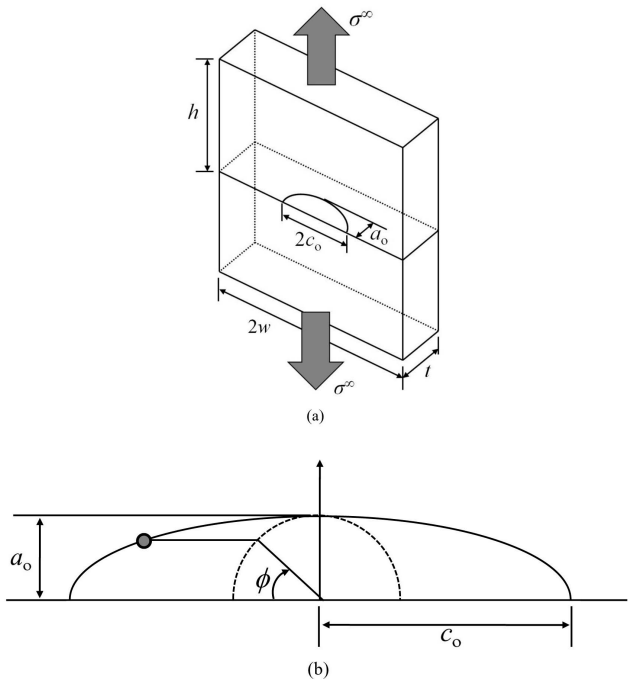

Fig. 4. (a) Schematic Illustration of Plate Containing Single Surface Crack Under Axial Tension and (b) Definition of the Crack Angle ϕ along the Crack Front

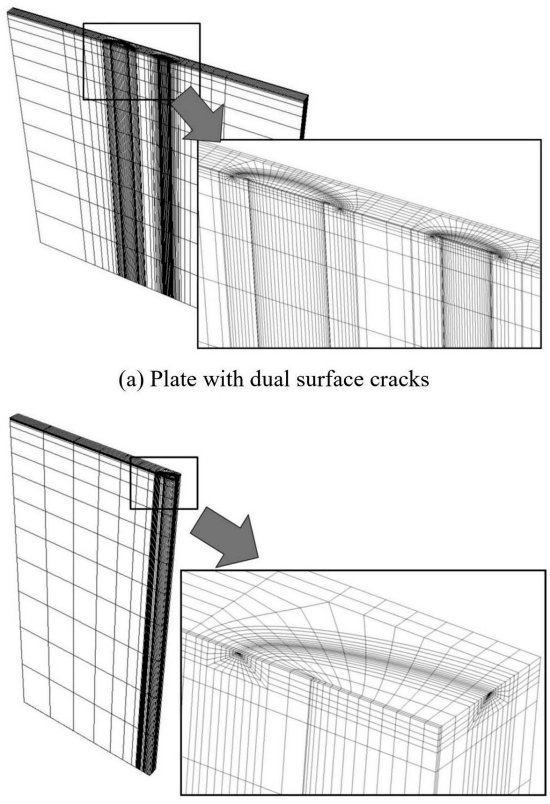

(a) Plate with dual surface cracks

(b) Plate with single surface crack

Fig. 5. Typical FE Meshes Employed in the Present Study

where J_e is the elastic J-integral, E is the Young's modulus, E=200GPa, and ν denotes the Poisson's ratio, ν=0.3. Note that a plane strain condition was assumed for calculating K from the elastic FE J values. Since the J-integral estimates at a free surface tend to be unreliable [12], the K values at the surface points were extrapolated using a fourth order polynomial fit near a free surface.

Furthermore, K can be expressed as

$$K = \sigma^{\infty} \sqrt{\pi c} F , \quad (5)$$

where σ^{∞} denotes the nominal stress acting on a remote surface of a plate and c is a half of the crack length. In Eq. (5), F denotes the shape factor for the elastic stress intensity factor. In general, K is defined using crack depth rather than crack length for a surface cracked component. However, in the present study, half of the crack length was employed to define an elastic stress intensity factor since the crack length was changed to quantify a crack interaction effect in the present study. However, as long as a consistent equation is used, this assumption does not affect the present stress intensity factor results. When calculating the F values along the crack front from the elastic FE J values using Eq. (5) for the plate with dual surface cracks, a crack length of c=c_1 was used for a larger crack, whereas c=c_2 was used for a smaller crack.

In order to validate the FE model employed in the present study, K values over a range of ϕ, resulting from the elastic FE results, were compared with the Raju-Newman solution results [13] for a_o/t=0.5 and c_o/a_o=3, which revealed good overall agreements along the crack front, as shown in Fig. 6. Thus, sufficient confidence in the present FE models and calculations was attained.

4. RESULTS AND DISCUSSION

The elastic stress intensity factors, the values of F resulting from Eq. (5), along the crack front for the plate with dual surface cracks for the case of c/a=3 are shown in Fig. 7 as a function of the angular location ϕ. The F values for the three different values of distance S were plotted (see Table 1). The F values of the single cracked plate of which the crack length is identical to that for the larger crack of the plate with dual surface cracks are also given in Fig. 7(a). Note again that the definition of the angular location ϕ is depicted in Fig. 2(b) for the plate

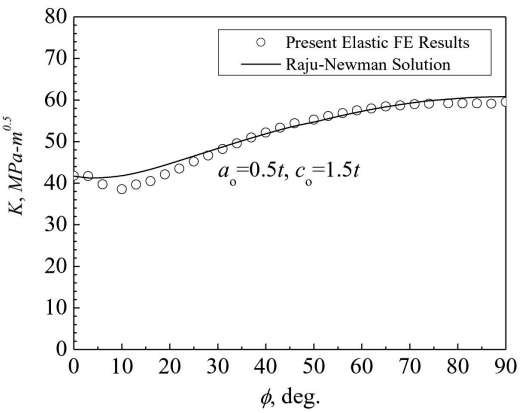

Fig. 6. Comparison of the FE K Values along the Crack Front from the Present FE Calculations with the Raju-Newman Solution

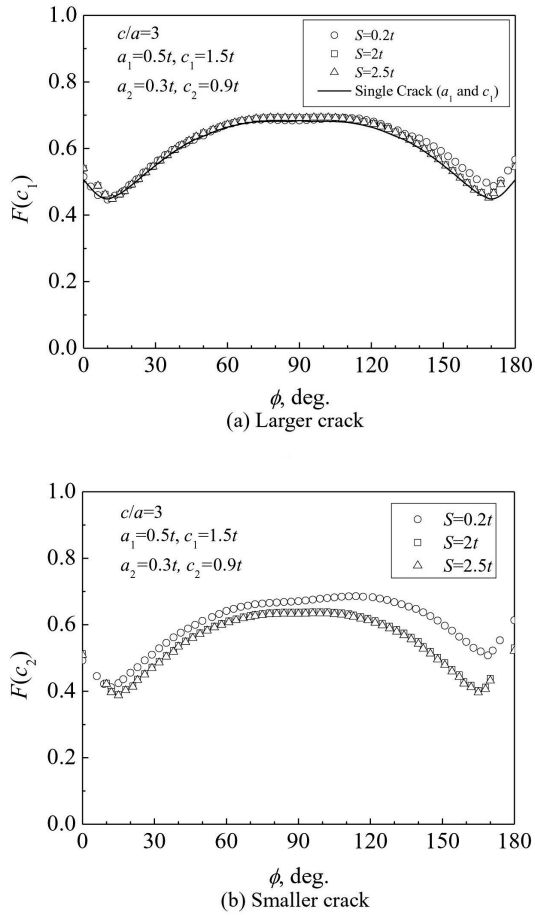

Fig. 7. Variation of the K Values along the Crack Front for the Case of c/a=3 (for the Larger Crack, K Values of the Single Crack are Also Given)

with dual surface cracks and in Fig. 4(b) for the plate with a single surface crack. As shown in Fig 7(a), the significance of the variations for the stress intensity factors is different at the locations along the crack front and is affected by the distance between the adjacent cracks, as expected. For a larger crack, the stress intensity factors are magnified along the crack front ranging from ϕ=120° to ϕ=180°, and the surface point (ϕ=180°) in the proximity of another crack yields a maximum interaction due to the adjacent crack. The change in the stress intensity factors increases due to the crack interaction effects as the distance between the adjacent cracks decreases. On the other hand, the interaction effects along the crack front ranging from ϕ=0° to ϕ=~120° are negligible, while the stress intensity factors of a smaller crack along the crack front are affected by the interaction effects for the whole crack-tip region as shown in Fig. 7(b), although the values of the stress intensity factor, K, for a larger crack are always larger than those of a smaller crack. As shown in Fig. 7(a), for the larger of dual surface cracks, the maximum value of the stress intensity factor is produced at the deepest point as revealed, but this value is not affected by the interaction effects due to the adjacent crack, i.e. the stress intensity factors of a crack front close to a surface point in proximity to another crack are only varied due to the crack interaction effects.

Figure 8 compares the elastic stress intensity factors along the crack front depending on the distance between the adjacent cracks for the case of c/a=1, i.e., a semi-circular shaped crack. The F values of the single cracked plate of which the crack length is identical to that for a larger crack of the plate with dual surface cracks are also given in Fig. 8(a). The overall tendency of the variation for the stress intensity factors due to a crack interaction is similar to that of c/a=3. For a larger crack, the variation of the stress intensity factor along the crack front ranging from ϕ=0° to ϕ=~120° is relatively small, while the stress intensity factors of a smaller crack are affected by a crack-tip interaction for the whole crack-tip region. In this case, a maximum interaction effect also appears at a surface point (ϕ=180°) in the proximity of another crack, and the interaction effects increase as the distance between two cracks decreases. In such cases, the maximum value of the stress intensity factor is typically produced at a surface point, and thus the maximum value is affected by the interaction effects in the case of a surface crack of a semi-circular shape, whereas the maximum value of the stress intensity factor for the case of c/a=3 is not varied since its deepest point is not affected by the interaction effects, as mentioned above.

The values of the elastic stress intensity factors along the crack front for the case of c/a=0.5 as a function of the distance between cracks are shown in Fig. 9. In the case of c/a=0.5, the crack interaction effects in proximity to an adjacent crack are not significant for the distances between cracks evaluated in the present study. However, some different trends could be found, i.e. contrary to expectations, the maximum interaction effect appears in the other side of larger crack, ϕ=0°. This trend seems to be due to the fact that, since in the present study the crack depth is fixed to be a_1/t=0.5 and a_2/t=0.3, the crack length of this case is shorter than in the previous 2 cases, and thus the stress field at ϕ=0° is affected by the deformation of the whole cracked area, which results in a more severe stress concentration at ϕ=0° than that at ϕ=180°. Figure 10 shows the von-Mises stress and crack opening stress distribution at the cracked region for the case of c/a=0.5 with S=0.2t. As shown in these figures, in the cases of c/a=0.5, the maximum stress is produced not at the surface point in proximity to the adjacent crack (ϕ=180°) but at the other surface point (ϕ=0°) of the larger crack, which

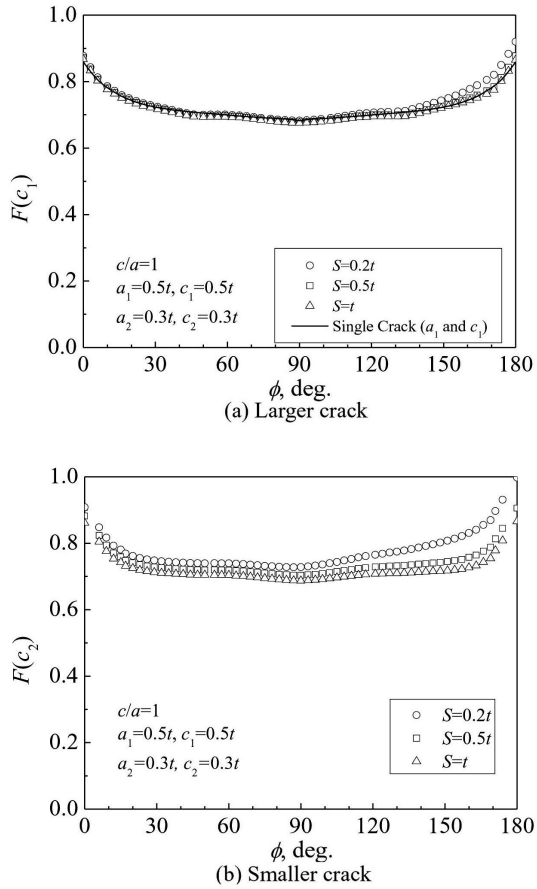

Fig. 8. Variation of the K Values along the Crack Front for the Case of c/a=1 (for the Larger Crack, K Values of the Single Crack are Also Given)

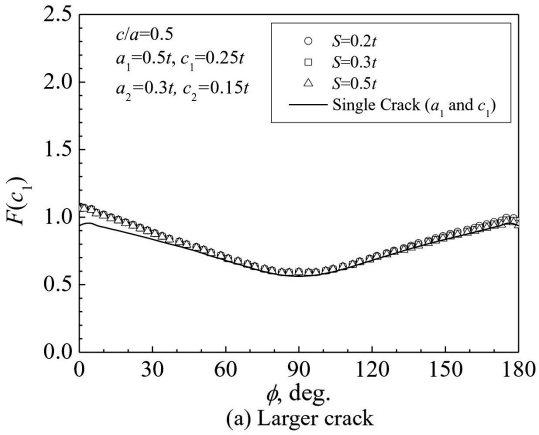

(a) Larger crack

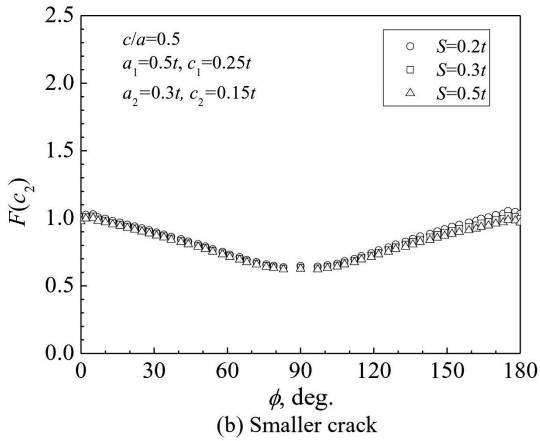

(b) Smaller crack

Fig. 9. Variation of the K Values along the Crack Front for the Case of c/a=0.5 (for the Larger Crack, K Values of the Single Crack are Also Given)

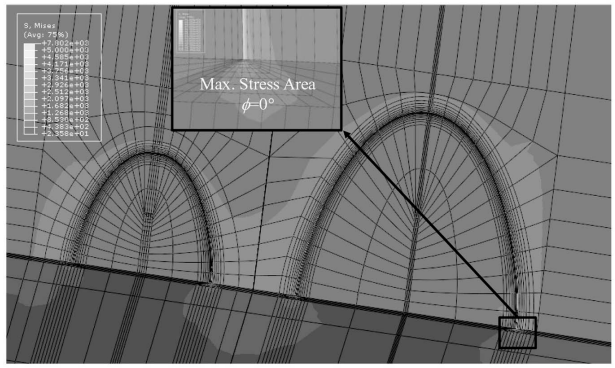

(a) von-Mises stress

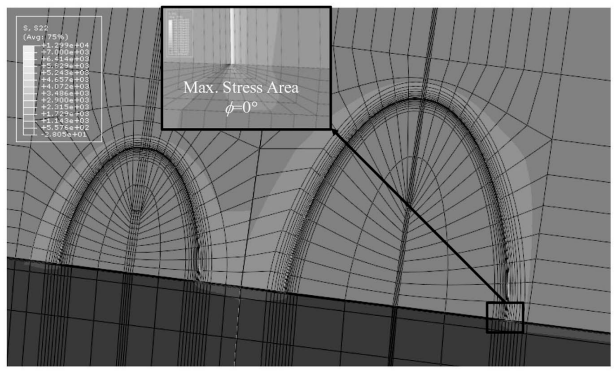

(b) Stress along the crack opening direction

Fig. 10. Stress Distribution at the Crack Tip for the Case of c/a=0.5

results in maximum stress concentration and interaction effect at ϕ=0° rather than ϕ=180°. The increases of the stress intensity factor due to the interaction effects at ϕ=0° are about 13% regardless of the S values, as shown in Fig. 9(a). However, for a smaller crack, the maximum interaction effect is generated at a surface point in proximity to the adjacent cracks, i.e. ϕ=180°, similarly to the previous cases. Based on the results from these three cases with different aspect ratios, it can be understood that the crack interaction effect can be significantly affected by the crack shape, i.e. the crack aspect ratio.

The ratio of the stress intensity factor at a surface point in the proximity of another crack (Point "A" defined at ϕ=180°, see Fig. 2(b)) of the plate with dual cracks to the stress intensity factor at a surface point of the plate with a single crack are compared in Fig. 11 as a function of the distance between cracks, and tabulated in Table 2. The distance between the adjacent cracks is normalized by the plate thickness, t. The values of the critical distance (S_{min}) for a crack combination into a new single crack

Table 2. Crack Interaction at Point "A"

c/a	S	Interaction at Point "A"
3	0.2t	1.119
	2t	1.079
	2.5t	1.074
1	0.2t	1.071
	0.5t	1.021
	t	1.007
0.5	0.2t	1.035
	0.3t	1.018
	0.5t	1.002

based on each combination rule are also shown in Fig. 11. In the *y*-axis of Fig. 11, the subscripts "dual" and "single" mean the shape factor, *F*, of the plate with dual surface cracks and with a single surface crack, respectively. As shown in Table 2 and Fig. 11, the increases in the stress intensity factor of the plate with dual surface cracks at its maximum interaction point (Point "A", see Fig. 2(b)) are around 7%~12% for the case of *c*/*a*=3 and 1%~7% for the case of *c*/*a*=1 when compared to the stress intensity factor for a single crack. As expected, the elevation of the stress intensity factor due to a crack interaction effect decreases as the distance between the cracks increases. In the case of *c*/*a*=0.5, the crack interaction effect at the surface point in the proximity of an adjacent crack is not significant for the distances between the cracks evaluated in the present study, whereas the increases of the stress intensity factor due to the interaction effects at ϕ=0° are about 13%. Note that the crack interaction effect at Point "A" decreases as the crack aspect ratio decreases. As mentioned above, the crack interaction effect at the deepest point of the larger crack is not significant. The stress intensity factors at the deepest point of the larger crack varied within a maximum difference of ~1% for *c*/*a*=3 and *c*/*a*=1, and within ~3% for *c*/*a*=0.5 when compared with the stress intensity factors at the deepest point of the single cracked plate.

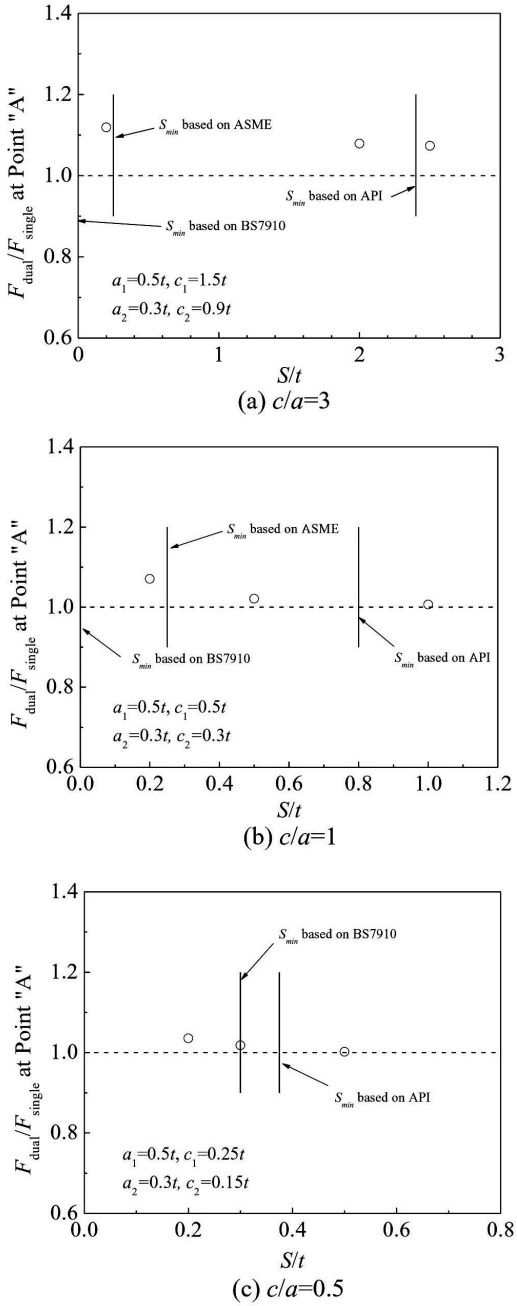

Fig. 11. Crack-Tip Interaction as a Function of the Distance Between Adjacent Cracks

As depicted in Fig. 11, the combination rule of API 579-1/ASME FFS-1 provides the most conservative results when compared with other rules. The combination rule of ASME Sec. XI also provides conservative criteria for the cases of *c*/*a*=3 and *c*/*a*=1. According to the findings of Ref. [8], the ASME code already allows an 18% to 25% increase in the stress intensity factor when assessing subsurface cracks. Thus, it can be argued that the maximum increases of 12% for *c*/*a*=3, 7% for *c*/*a*=1 and 13% for *c*/*a*=0.5 in the present study are also acceptable; in addition, the critical distance between cracks based on the ASME Sec. XI can be shortened further. On the other hand, the combination rule based on BS7910 (and R6) provides an appropriate guide for a crack interaction effect, although it also seems to be conservative for the case of *c*/*a*=0.5.

Figure 12 shows the elastic-plastic *J*-integral results for the case of *c*/*a*=3 considered in the present study. In this figure, the *J*-integral is normalized with respect to the material yield strength and for half of the crack length. The *J*-integral values are calculated along the crack front. Although only the results for *c*/*a*=3 are given in the present paper, in fact, the overall tendency of the elastic-plastic analyses results is identical to that of the elastic analyses results regardless of values of *c*/*a*. The *J*-integral values are also magnified along the crack front ranging from ϕ=110° to ϕ=180° for a larger crack, and a maximum interaction is found at the surface point (ϕ=180°), while the maximum value of the *J*-integral takes place at the deepest point, as is also the case for the elastic analysis. For a smaller crack, the range affected by the interaction effect is extended from ϕ=0° to ϕ=180°, which is also identical to the elastic analysis results. As shown in Fig. 12, the interaction effect also increases as the distance between two cracks decreases. Thus, it could be concluded that the interaction behavior of elastic-plastic materials is similar to that of elastic materials.

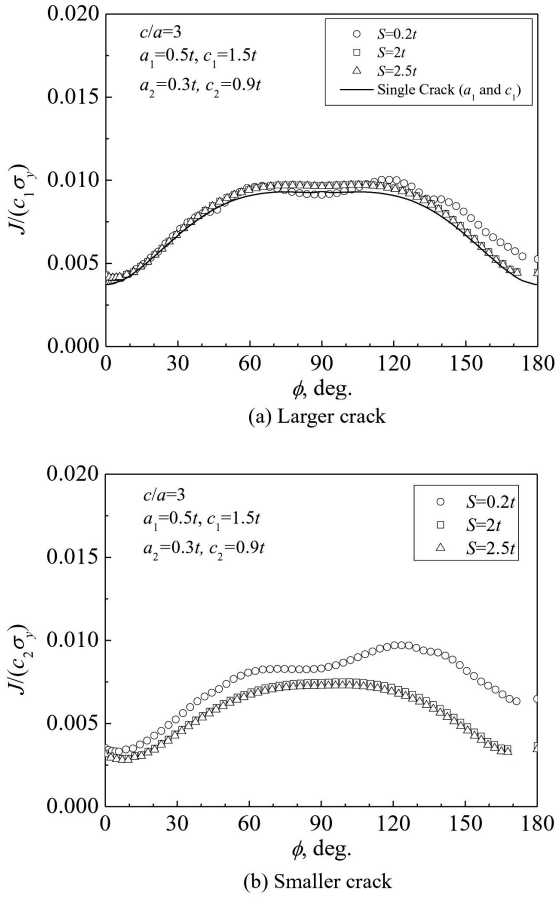

Fig. 12. Variation of the J Values along the Crack Front for the Case of c/a=3 at $\sigma^{\infty}=\sigma_y$ (for the Larger Crack, J Values of the Single Crack are Also Given)

5. CONCLUDING REMARKS

In the present study, the crack interaction effects of multiple in-plane surface cracks were investigated by evaluating the elastic stress intensity factors and the elastic-plastic J-integral along the crack front through detailed 3-D FE analyses. The effects on the fracture mechanics assessment parameters of the geometric parameters, the relative distance between adjacent cracks, and the crack aspect ratio were investigated systematically. The increase of these fracture mechanics assessment parameters at the maximum interaction point as a function of the distance between the cracks was estimated, which was evaluated with respect to the current crack combination rules to elucidate the most relevant guidance for crack interactions.

Based on the present results, all combination rules of current assessment codes reviewed in this study provide very conservative results compared to the allowable increase in the ASME code when assessing subsurface cracks. Based on this observation, it can be concluded that BS7910 seems to provide a relevant crack combination rule for in-plane dual surface cracks, whereas API 579-1/ASME FFS-1 provides the most conservative results. For a deeper crack, all the codes provide a very conservative rule. In particular, ASME Sec. XI still seems to have some room for a revision to shorten the critical distance between two adjacent cracks for a crack combination.

REFERENCES

[1] J. R. Rice, 1968, "A Path Independent Integral and the Approximate Analysis of Strain Concentration by Notches and Cracks," Journal of Applied Mechanics, Vol. 35, pp. 379~386.
[2] ASME, 2007, "Rules for In-Service Inspection of Nuclear Power Plant Components," ASME Sec. XI, Division 1, IWA-3000.
[3] American Petroleum Institute, 2007, "Fitness-for-Service," API 579-1/ASME FFS-1.
[4] British Standard Institute, 1999, "Guide on Methods for Assessing the Acceptability of Flaws in Fusion Welded Structures," BS7910, London.
[5] British Energy, 2001, "R6: Assessment of the Integrity of Structures Containing Defects," Revision 4.
[6] Y. Murakami and S. Nemat-Nsasser, 1982, "Interacting Disssimilar Semi-Elliptical Surface Flaws under Tension and Bending," Engineering Fracture Mechanics, Vol. 16, pp. 373~386.
[7] T. Miyoshi, M. Shiratori and O. Tanabe, 1985, "Stress Intensity Factors for Surface Cracks with Arbitrary Shapes in Plates and Shells," Fracture Mechanics: Sixteenth Symposium, ASTM STP 868, M.F. Kanninen and A.T. Hopper, Eds., American Society for Testing and Materials, Philadelphia, pp. 521~534.
[8] K. Hasegawa, K. Miyazaki and S. Kanno, 2001, "Interaction Criteria for Multiple Flaws on the basis of Stress Intensity Factors," ASME Pressure Vessels and Piping Conference, Vol. 422, pp. 23~29.
[9] M. Kamaya, 2005, "Influence of the Interaction on Stress Intensity Factor of Semi-Elliptical Surface Cracks," ASME Pressure Vessels and Piping Conference, PVP2005-71352.
[10] N. S. Huh, D. J. Shim, S. Choi, G. M. Wilkowski and J. S. Yang, 2008, "Stress Intensity Factors for Slanted Through-Wall Cracks based on Elastic Finite Element Analyses," Fatigue and Fracture of Engineering Materials and Structures, Vol. 31, pp. 197~208.
[11] ABAQUS, Inc., "User's Manual," ABAQUS Version 6.7-1, 2007.
[12] T. Nakamura and D. M. Parks, 1991, "Determination of Elastic T-Stress along 3-D Crack Fronts using an Interaction Integral," International Journal of Solids and Structures, Vol. 29, pp. 1597~1611.
[13] I. S. Raju and J. C. Newman, 1979, "Stress Intensity Factors for a Wide Range of Semi-Elliptical Surface Cracks in Finite-Thickness Plates," Engineering Fracture Mechanics, Vol. 11, pp. 817~829; see also T. Fett and D. Munz, 1997, "Stress Intensity Factors and Weight Functions," Computational Mechanics Publications.